Wave-equation tomography for anisotropic parameters

Yunyue (Elita) Li and Biondo Biondi

ABSTRACT

Anisotropic models are recognized as more realistic representations of the subsurface where complex geological environment exists. These models are widely needed by many anisotropic migration and interpretation schemes. However, anisotropic model building is still a challenging problem in the industry. In this paper, we propose an approach to build the anisotropic model using Wave-Equation Tomography (WETom) on surface seismic data in the image space. To reduce the null space of the inversion, we parametrize our model space using only vertical velocity (V_V) and the anellipticity parameter η. Numerical tests show that anisotropic WETom is effective in resolving model perturbations; however, ambiguity exists between the vertical velocity and the anellipticity parameter. Auxiliary information is needed to further constrain the inversion.

INTRODUCTION

Since first reported in exploration seismology in the 1930s (McCollum and Snell, 1932), the importance of anisotropy has been continuously increased in seismic imaging and exploration. This is partially due to acquisition with increasingly longer offsets and exploration in areas with strong geological deformation. Until now, the transverse isotropic (TI) model has been the most commonly used anisotropic model in seismic imaging. Postma (1955) and Helbig (1956) showed that a sequence of isotropic layers on a scale much smaller than the wavelength leads to an anisotropic medium. For the case of horizontal layers, the medium can be described by an equivalent vertical transverse isotropic (VTI) medium. When dip is present, the medium develops a tilted transverse anisotropy (TTI). Many authors (Shan, 2009; Fletcher et al., 2009; Zhang and Zhang, 2009; Fei and Liner, 2008) have developed various migration and processing schemes for VTI and TTI medium; however, the estimation of the anisotropy model is still challenging.

The existing anisotropic model-building schemes are mostly based on measuring the non-hyperbolic moveout along the traveltime curve to flatten the common image gathers (CIG) (Zhou et al., 2003, 2004; Yuan et al., 2006; Cai et al., 2009). However, traveltime-based methods are prone to errors and unrealistic results when multi-pathing exists in areas of complex overburden.

Wave-equation tomography (WETom) has been widely investigated in isotropic velocity building, and can be implemented either in the data space (Tarantola, 1984; Woodward, 1992) or in the image space (Sava and Biondi, 2004a,b; Shen, 2004; Shen and Symes, 2008; Guerra et al., 2009). Several advantages drive us to use the image-space WETom instead of the data-space version: First, the migration image is often much cleaner than the recorded wavefields. Second, we can use cheaper one-way extrapolators in the image space, compared with expensive two-way extrapolators in the data space. Third, the objective function is directly related to the final image. Therefore, we choose to extend image-space WETom from isotropic velocity building to anisotropic model building.

In this paper, we first explain the parametrization of the inversion problem and then extend image-space WETom from the isotropic medium to the anisotropic medium. We show that theoretically the gradient of the tomographic objective functional for the anisotropic medium is similar to its isotropic version, with an extra term for the additional parameter. Then, we test the anisotropic WETom operator using a model with a localized anomaly. Finally, we invert for a 2-D VTI model using the proposed anisotropic WETom operator.

PARAMETERIZATION

In the VTI medium, Thomsen parameters ϵ and δ are commonly used to characterize the anisotropic seismic velocity. These two parameters define the relationships between the vertical velocity (V_V), the horizontal velocity (V_H), and the NMO velocity (V_N) as follows:

$$V_H^2 = V_V^2(1+2\epsilon), \tag{1}$$

$$V_N^2 = V_V^2(1+2\delta). \tag{2}$$

In the practice of surface seismic exploration, it is impossible to estimate the vertical velocity because depth of the reflectors is unknown, and there is no vertical offset information in the data. However, if we have long enough in-line and cross-line offsets, it may be possible to resolve the horizontal velocity and the NMO velocity. Therefore, the anellipticity parameter η is used to provide a direct link between V_N and V_H:

$$V_H^2 = V_N^2(1+2\eta), \tag{3}$$

where η is defined by the Thomsen parameters as follows:

$$\eta = \frac{\epsilon-\delta}{(1+2\delta)}. \tag{4}$$

To reduce the number of parameters, and thereby the null space of the resulting inversion procedure, we make an arbitrary assumption that $\delta = 0$. Hence, there are

only two independent parameters:

$$\eta \;=\; \epsilon \tag{5}$$

and

$$V_V \;=\; V_N. \tag{6}$$

Therefore, we choose to use V_V and η as the model parameters that we will estimate during the inversion.

WETOM FOR ANISOTROPIC PARAMETERS

Anisotropic WETom is a non-linear inversion process that aims to find the anisotropic model that minimizes the residual field $\Delta\mathbf{I}$ in the image space. The residual image is derived from the background image $\mathbf{I}$, which is computed with current background model. In general, the residual image is defined as (Biondi, 2008)

$$\Delta\mathbf{I} = \mathbf{I} - \mathbf{F}(\mathbf{I}), \tag{7}$$

where $\mathbf{F}$ is a focusing operator acting on the background image.

In the least-squares sense, the tomographic objective function can be written as follows:

$$J = \frac{1}{2}||\Delta\mathbf{I}||_2 = \frac{1}{2}||\mathbf{I} - \mathbf{F}(\mathbf{I})||^2. \tag{8}$$

To perform the WETom for anisotropic parameters, we first need to extend the tomographic operator from the isotropic medium (Shen, 2004; Sava, 2004; Guerra et al., 2009) to the anisotropic medium. We define the image-space wave-equation tomographic operator $\mathbf{T}$ for anisotropic parameters as follows:

$$\begin{aligned} \mathbf{T} &= \left.\frac{\partial \mathbf{I}}{\partial \mathbf{m}}\right|_{\mathbf{m}=\widehat{\mathbf{m}}} \\ &= \left.\frac{\partial \mathbf{I}}{\partial \mathbf{s}}\right|_{\mathbf{s}=\widehat{\mathbf{s}}} + \left.\frac{\partial \mathbf{I}}{\partial \eta}\right|_{\eta=\widehat{\eta}}, \end{aligned} \tag{9}$$

where $\mathbf{m}$ is the anisotropy model, which in this case includes vertical slowness $\mathbf{s}$ and anellipticity parameter η; $\widehat{\mathbf{m}}$ is the background anisotropy model, consisting of the background slowness $\widehat{\mathbf{s}}$ and background anellipticity $\widehat{\eta}$; $\mathbf{I}$ is the image. This WETom operator $\mathbf{T}$ is a linear operator that relates the model perturbation $\Delta\mathbf{m}$ to the image perturbation $\Delta\mathbf{I}$ as follows:

$$\Delta\mathbf{I} = \mathbf{T}\Delta\mathbf{m}. \tag{10}$$

In this paper, we evaluate the anisotropic tomographic operator in the shot-profile domain.

Both source and receiver wavefields are downward continued in the shot-profile domain using the one-way wave equations (Claerbout, 1971):

$$\begin{cases} \left(\frac{\partial}{\partial z} + i\Lambda\right) D(\mathbf{x}, \mathbf{x}_s) = 0 \\ D(x, y, z = 0, \mathbf{x}_s) = f_s \delta(\mathbf{x} - \mathbf{x}_s) \end{cases}, \tag{11}$$

and

$$\begin{cases} \left(\frac{\partial}{\partial z} - i\Lambda\right) U(\mathbf{x}, \mathbf{x}_s) = 0 \\ U(x, y, z = 0, \mathbf{x}_s) = Q(x, y, z = 0, \mathbf{x}_s) \end{cases}, \tag{12}$$

where $D(\mathbf{x}, \mathbf{x}_s)$ is the source wavefield at the image point $\mathbf{x} = (x, y, z)$ with the source located at $\mathbf{x}_s = (x_s, y_s, 0)$; $U(\mathbf{x}, \mathbf{x}_s)$ is the receiver wavefield at the image point $\mathbf{x}$ with the source located at $\mathbf{x}_s$; f_s is the source signature, and $f_s\delta(\mathbf{x} - \mathbf{x}_s)$ defines the point source function at $\mathbf{x_s}$, which serves as the boundary condition of Equation 11; $Q(x, y, z = 0, \mathbf{x}_s)$ is the recorded shot gather at $\mathbf{x}_s$, which serves as the boundary condition of Equation 12. Operator Λ is the dispersion relationship for anisotropic wave propogation:

$$\Lambda = \omega s(\mathbf{x}) \sqrt{1 - \frac{|\mathbf{k}|^2}{\omega^2 s^2(\mathbf{x}) - 2\eta(\mathbf{x})|\mathbf{k}|^2}}, \tag{13}$$

where ω is the angular frequency, $s(\mathbf{x})$ is the slowness at $\mathbf{x}$, $\eta(\mathbf{x})$ is the anellipticity at $\mathbf{x}$; $\mathbf{k} = (k_x, k_y)$ is the spatial wavenumber vector. Dispersion relationship 13 can be approximated with a rational function by Taylor series and Padé expansion analysis (Shan, 2009):

$$\Lambda = \omega s(\mathbf{x})(1 - \frac{a|\mathbf{k}|^2}{\omega^2 s^2(\mathbf{x}) - b|\mathbf{k}|^2}) \tag{14}$$

where, to the second order, $a = 0.5, b = 2\eta + 0.25$. Using binomial expansion, Equation 14 can be further expanded to polynomials:

$$\Lambda = \omega s(\mathbf{x}) - \frac{a}{\omega s^2(\mathbf{x})}|\mathbf{k}|^2 - \frac{3ab}{\omega^3 s^4(\mathbf{x})}|\mathbf{k}|^4. \tag{15}$$

The background image is computed by applying the cross-correlation imaging condition:

$$I(\mathbf{x}, \mathbf{h}) = \sum_{\mathbf{x}_s} \sum_{\omega} \overline{D(\mathbf{x} - \mathbf{h}, \mathbf{x}_s)} U(\mathbf{x} + \mathbf{h}, \mathbf{x}_s), \tag{16}$$

where the overline stands for the complex conjugate, and $\mathbf{h} = (h_x, h_y, h_z)$ is the subsurface half-offset.

Under the Born approximation, a perturbation in the model parameters causes a first-order perturbation in the wavefields. Consequently, the resulting image perturbation reads:

$$\begin{aligned} \Delta I(\mathbf{x}, \mathbf{h}) \;=\; & \sum_{\mathbf{x}_s} \sum_{\omega} \Big(\overline{\Delta D(\mathbf{x} - \mathbf{h}, \mathbf{x}_s)} \widehat{U}(\mathbf{x} + \mathbf{h}, \mathbf{x}_s) + \\ & \overline{\widehat{D}(\mathbf{x} - \mathbf{h}, \mathbf{x}_s)} \Delta U(\mathbf{x} + \mathbf{h}, \mathbf{x}_s) \Big), \end{aligned} \tag{17}$$

where $\widehat{D}(\mathbf{x}-\mathbf{h}, \mathbf{x}_s)$ and $\widehat{U}(\mathbf{x}+\mathbf{h}, \mathbf{x}_s)$ are the background source and receiver wavefields computed with the background model $\widehat{m}(\mathbf{x})$, $\Delta D(\mathbf{x} - \mathbf{h}, \mathbf{x}_s)$ and $\Delta U(\mathbf{x} + \mathbf{h}, \mathbf{x}_s)$ are

the perturbed source wavefield and perturbed receiver wavefield, respectively, which result from the model perturbation $\Delta m(\mathbf{x})$.

To evaluate the adjoint tomographic operator $\mathbf{T}^*$, which backprojects the image perturbation into the model space, we first compute the wavefield perturbation from the image perturbation using the adjoint imaging condition:

$$\begin{aligned} \Delta D(\mathbf{x},\mathbf{x}_s) &= \sum_{\mathbf{h}} \Delta I(\mathbf{x},\mathbf{h}) \widehat{U}(\mathbf{x}+\mathbf{h},\mathbf{x}_s) \\ \Delta U(\mathbf{x},\mathbf{x}_s) &= \sum_{\mathbf{h}} \Delta I(\mathbf{x},\mathbf{h}) \widehat{D}(\mathbf{x}-\mathbf{h},\mathbf{x}_s). \end{aligned} \tag{18}$$

The perturbed source and receiver wavefields satisfy the following one-way wave equations, linearized with respect to slowness and η:

$$\begin{cases} \left(\frac{\partial}{\partial z} + i\Lambda\right) \Delta D(\mathbf{x},\mathbf{x}_s) = \left(-i\frac{\partial \Lambda}{\partial \mathbf{m}} \widehat{D}(\mathbf{x},\mathbf{x}_s)\right) \Delta \mathbf{m}^*(\mathbf{x}) \\ \Delta D(x,y,z=0,\mathbf{x}_s) = 0 \end{cases}, \tag{19}$$

and

$$\begin{cases} \left(\frac{\partial}{\partial z} - i\Lambda\right) \Delta U(\mathbf{x},\mathbf{x}_s) = \left(-i\frac{\partial \Lambda}{\partial \mathbf{m}} \widehat{U}(\mathbf{x},\mathbf{x}_s)\right) \Delta \mathbf{m}^*(\mathbf{x}) \\ \Delta U(x,y,z=0,\mathbf{x}_s) = 0 \end{cases}, \tag{20}$$

where $\mathbf{m}$ is the row vector $[\mathbf{s}\ \eta]$, and $\mathbf{m}^*$ is the transpose of $\mathbf{m}$.

When solving the optimization problem, we obtain the image perturbation by migrating the data with the current background model and performing a focusing operation (Equation 7). Then the perturbed image is convolved with the background wavefields to get the perturbed wavefields (Equation 18). The scattered wavefields are computed by applying the adjoint of the one-way wave-equations 19 and 20. Finally, the model space gradient is obtained by cross-correlating the upward propagated scattered wavefields with the modified background wavefields (terms in the parentheses on the right-hand sides of Equations 19 and 20).

NUMERICAL TEST OF THE ANISOTROPIC WETOM OPERATOR

To test the anisotropic WETom operator, we run the forward and adjoint WETom operator on a 2-D model. Figure 1 shows the background isotropic model, with one reflector in velocity and no anisotropy. The data are modeled with 4000m maximum offset, 8m receiver spacing, 80m source spacing and 41 split-spread shots. We use the two-way acoustic anisotropic modeling code in Madagascar to do the modeling, and the one-way SSF (Tang and Clapp, 2006) extrapolator to do the migration.

Figure 2 shows the model perturbations, with a rectangular slowness anomaly that is 10% lower than the background slowness on the left, and a rectangular anisotropic

anomaly on the right. The perturbation in η within the rectangular block is constant ($\Delta\eta = 0.1$). Figure 3 shows the perturbed image at the zero lag of the subsurface offset due to the model perturbations after applying the forward WETom operator. Adjoint WETom operator back-projects the perturbed image into the model space, and outputs the gradient for the model perturbation, as shown in Figure 4. Comparing Figure 2 and Figure 4, we can see that the gradients provide the correct direction and shape of the perturbation to conduct a line search in a given inversion scheme.

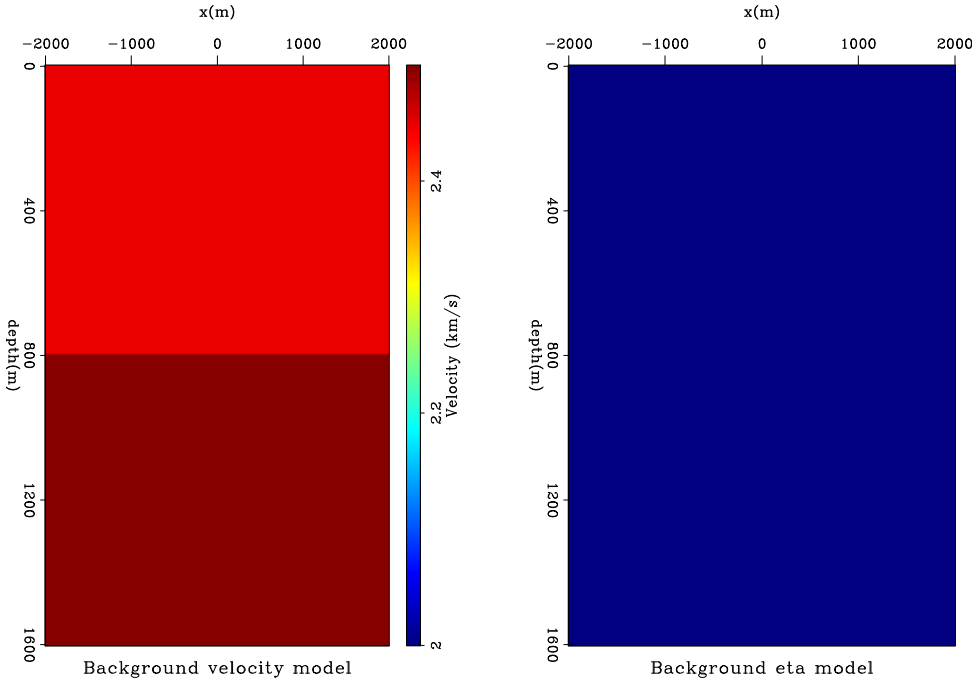

Figure 1: Background isotropic model. Left is the velocity model with one reflector, and right is the η model with constant zero. [**ER**]

INVERSION FOR 2-D VTI MODELS

From the gradient given by the anisotropic WETom operator in last section, we notice that the perturbations in slowness and η are co-located. This is an intrinsic characteristic of the operator, which may not be geologically realistic. Therefore, we design three tests to examine this effect in the inversion.

In these three tests, we use the same initial model (Figure 5), but data modeled using different true models. In Figure 6 we show the true model perturbations, which have one layer of perturbations in slowness only, in η only, and in both. Figure 7 shows the angle-domain common image gathers (ADCIGs) using the initial model, where ADCIGs are not flat due to the error in the model. Notice the image perturbation is small for the perturbation in η only.

In the inversion, we define the focusing operator in the perturbed image (Equation

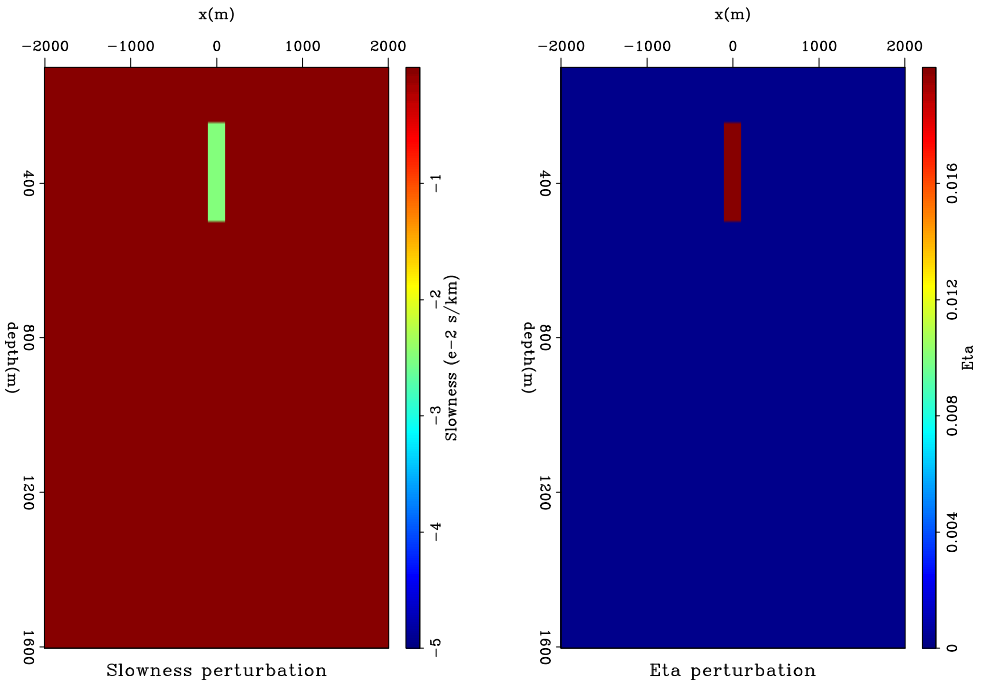

Figure 2: Model perturbations. Left is a rectangular slowness anomaly that is 10% lower than the background slowness , and right is a rectangular anisotropic anomaly with a constant value of $\Delta\eta = 0.1$. [**ER**]

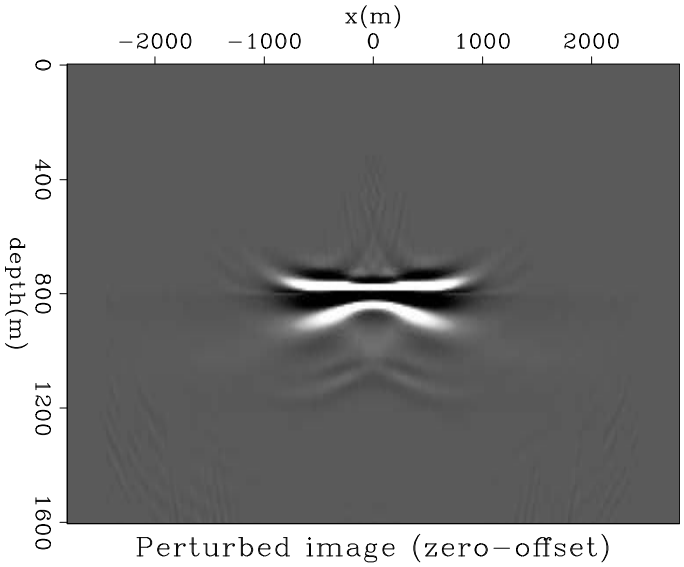

Figure 3: Perturbed image from the forward anisotropic WETom operator. The image is extracted from the zero lag of the subsurface offset. [**ER**]

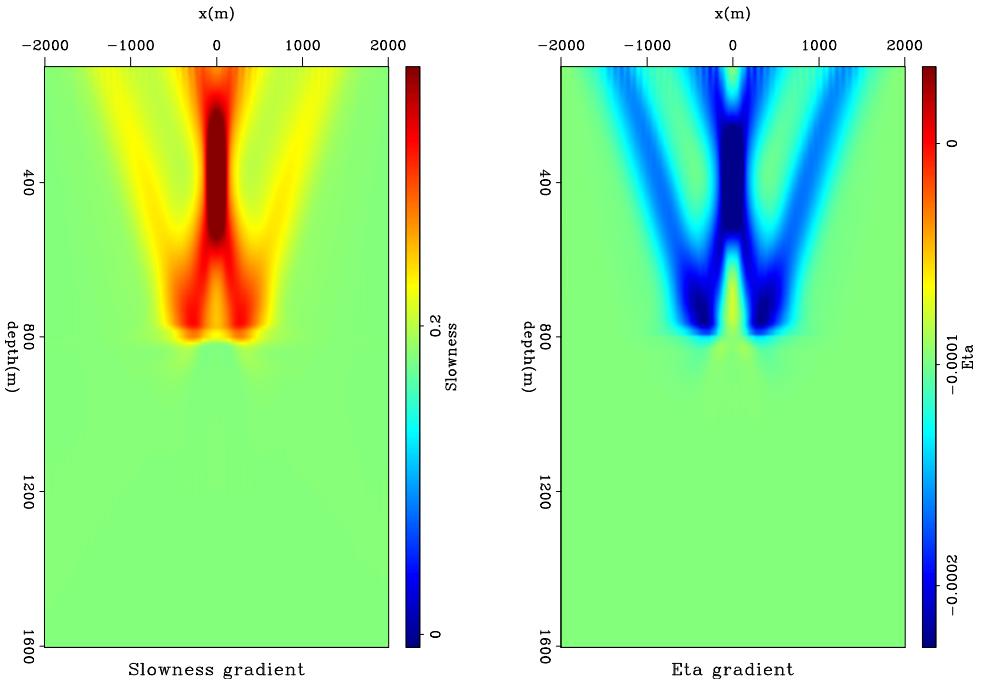

Figure 4: Back-resolved gradient for the model updates. Left is the gradient for slowness, and right is the gradient for η. [**ER**]

7) by the Differential Semblance Optimization (DSO) method (Shen, 2004):

$$\mathbf{F}(\mathbf{I}) = (\mathbf{1} - \mathbf{O})\mathbf{I}, \tag{21}$$

where $\mathbf{1}$ is the identity operator and $\mathbf{O}$ is the DSO operator. Therefore, the objective function (Equation 8) becomes:

$$J = \frac{1}{2}||\mathbf{O}\widehat{\mathbf{I}}||^2 = \frac{1}{2}||h\widehat{\mathbf{I}}||^2, \tag{22}$$

where h is the subsurface half-offset. Since the DSO operator is independent of the model parameters, the gradient of J with respect to the model parameters is

$$\nabla J = \left(\frac{\partial \mathbf{I}}{\partial \mathbf{m}}\bigg|_{\mathbf{m}=\widehat{\mathbf{m}}}\right)^* \mathbf{O}^*\mathbf{O}\widehat{\mathbf{I}} = \mathbf{T}^*\mathbf{O}^*\mathbf{O}\widehat{\mathbf{I}}. \tag{23}$$

To minimize the objective function, we specifically use the steepest descent algorithm. To help convergence, we average the gradient at each depth to ensure a layered model and mute the shallow updates to avoid near-surface artifacts.

Figure 8 shows the final model updates after 4 non-linear iterations. The results should be comparable to the model perturbations in Figure 6. In the final updates, we see a consistent over predition of η. This is because error in η has a very smal contribution in the image perturbation, as shown in the middle panel of Figure 7. Figure 9 shows the ADCIGs using the updated model. Comparing Figure 6 and Figure

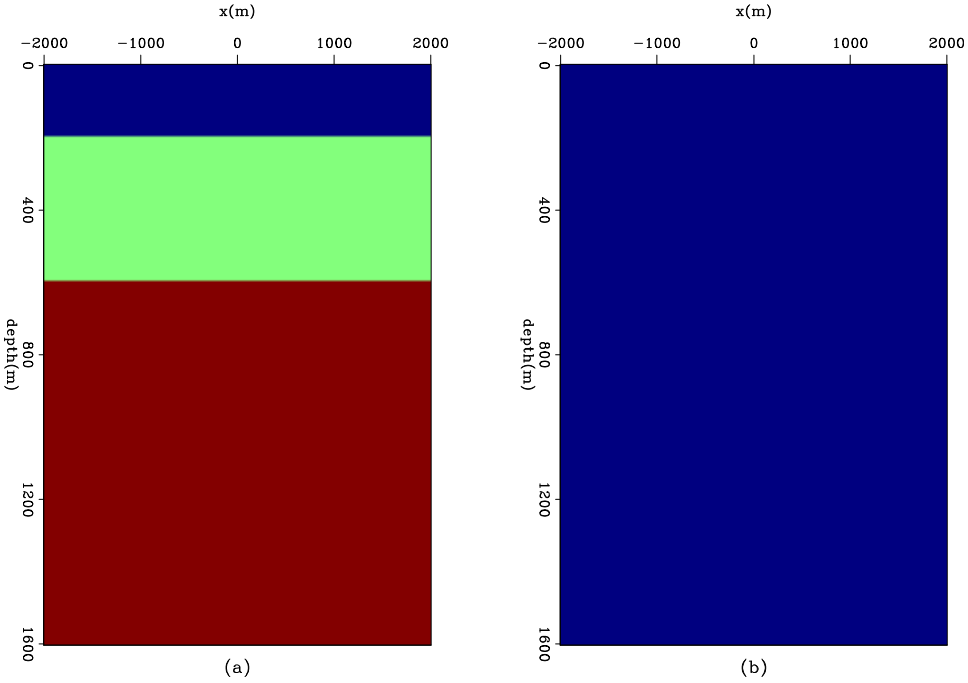

Figure 5: Initial model for inversion. Panel (a) is the initial velocity model with three layers; Panel (b) is the initial η model with constant value of zero. [**ER**]

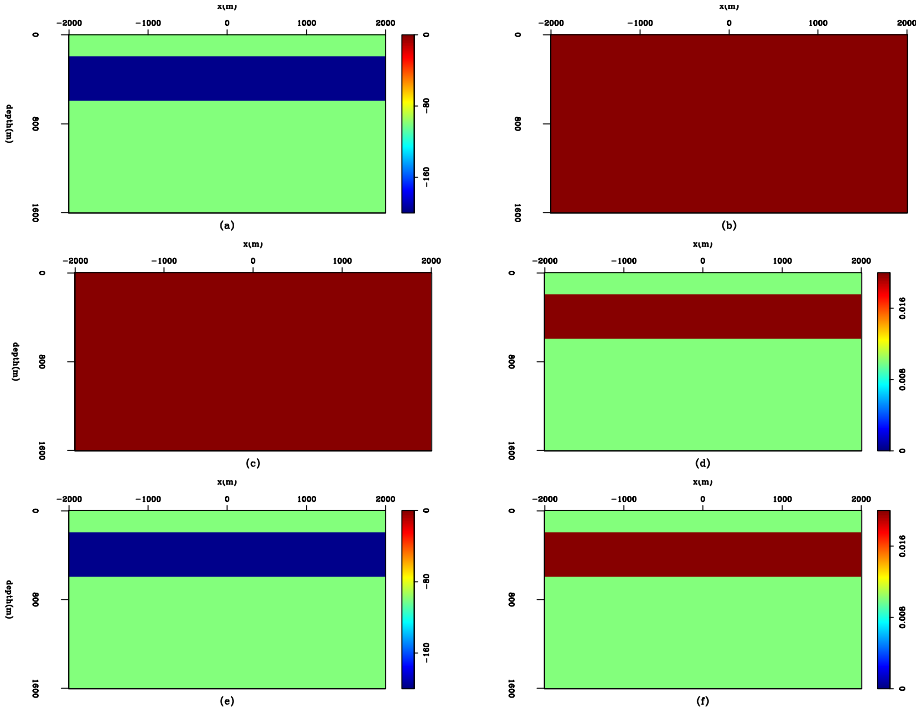

Figure 6: True model perturbation in three test cases. Panel (a) and (b): Perturbation in velocity only; Panel (c) and Panel (d): Perturbation in η only; Panel (e) and Panel (f): Perturbations in both. [**ER**]

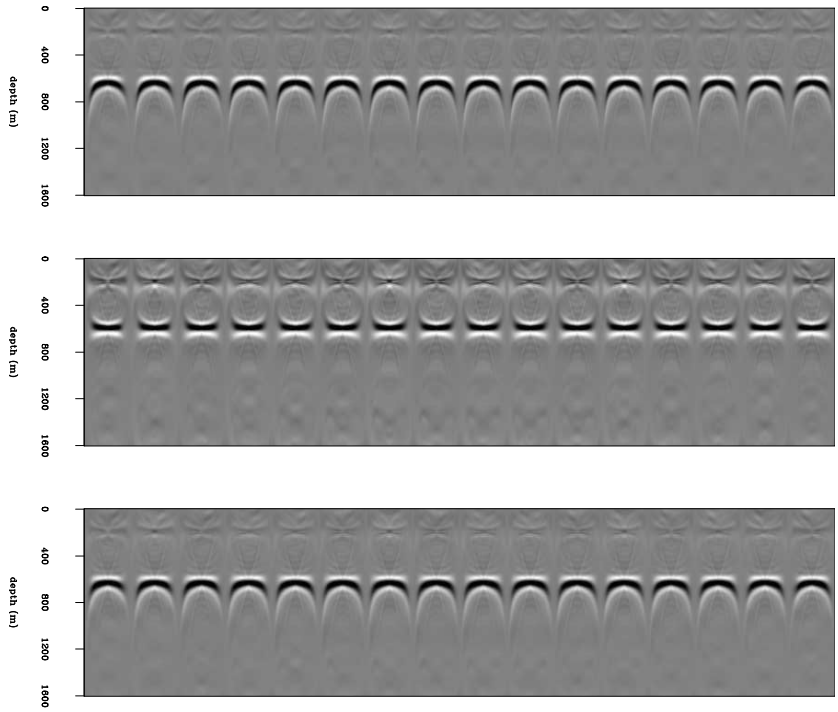

Figure 7: ADCIGs using the initial model in three cases. Top panel: Perturbation in velocity only; Middle panel: Perturbation in η only; Bottom panel: Perturbations in both. Curvature in the ADCIGs indicates errors in velocity or η. [**ER**]

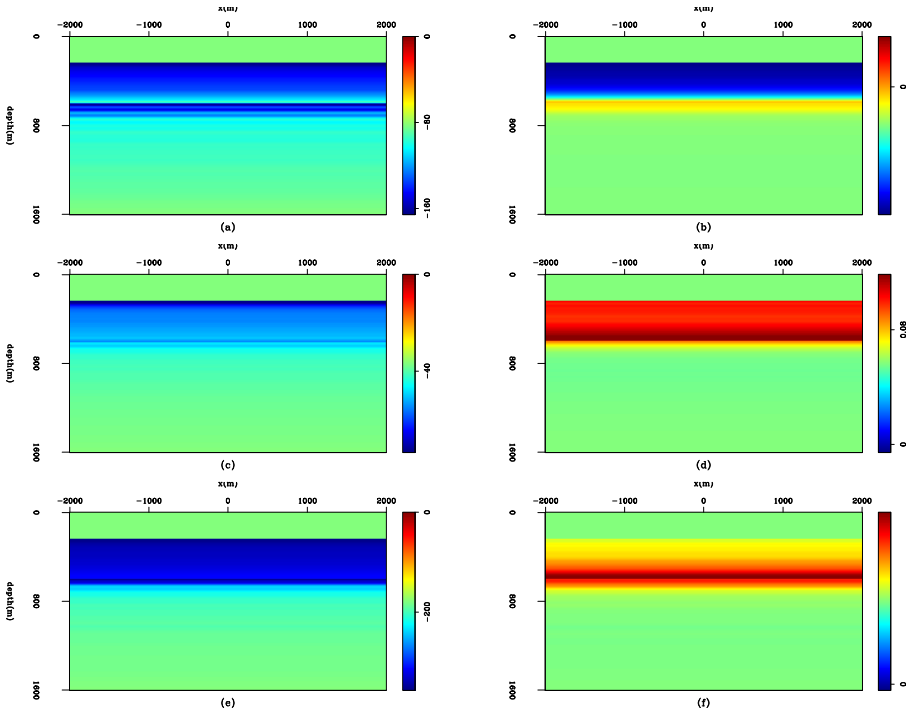

Figure 8: Inversion results of the three test cases. Panels are comparable to those in Figure 6. [**CR**]

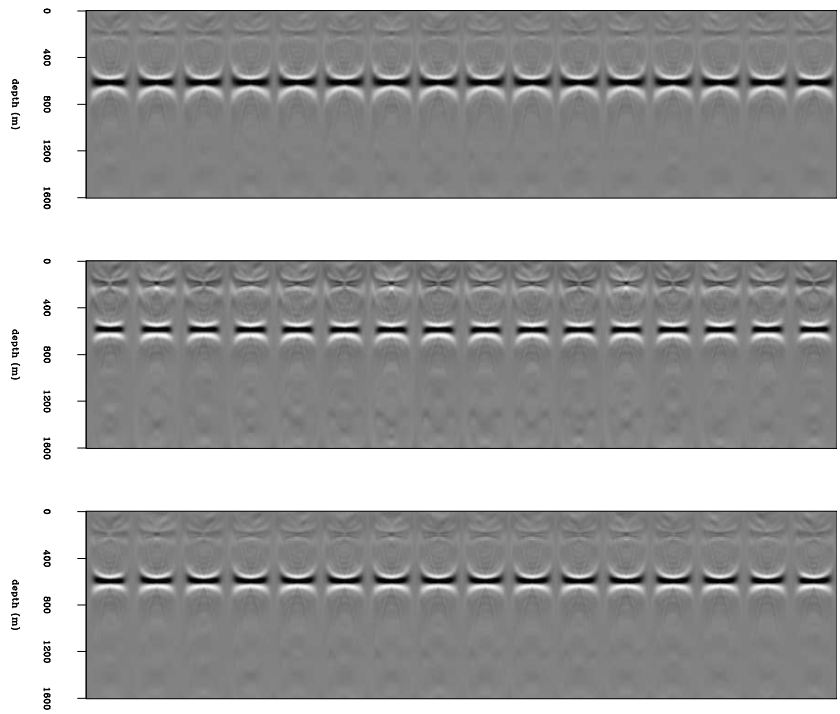

Figure 9: Common image gathers using the updated model in three cases. Top panel: Perturbation in velocity only; Middle panel: Perturbation in η only; Bottom panel: Perturbations in both. ADCIGs are flattened compared with Figure 7. [**ER**]

8, Figure 7 with Figure 9, we can conclude that the inversion successfully identifies the layered perturbation and flattens the ADCIGs. However, back-projection of the residual image shows up in both parameter spaces, although it is caused by perturbations in a single parameter. Also for the case of perturbing both spaces, the over-prediction of velocity perturbation and the under-prediction of η perturbation reconcile with each other and produce flat events in the ADCIGs. Therefore, we can conclude that the ambiguity between the velocity and the anellipticity cannot be resolved simply by the inversion, and auxiliary information is needed to further distinguish the difference.

CONCLUSIONS AND DISCUSSION

In this paper, we present a novel method to build the anisotropic velocity model using image-space wave-equation tomography. The mathematical formulation of the operator shows that by adding an additional term for η, the gradient of the anisotropic WETom shows similar structure as that for the isotropic case. Our numerical tests show that the anisotropic WETom operator is useful in identifying both localized and layered perturbation in simple cases. However, when only one parameter is perturbed, the WETom operator produces a model with perturbations in both parameters.

One possible way to resolve this ambiguity is to utilize the moveout information in the subsurface offset domain and/or angle domain. It has been shown that the RMO functions are different in ADCIGs for isotropic perturbations (Biondi and Symes, 2004) and anisotropic perturbations (Biondi, 2007). Therefore, adding the RMO information may help to distinguish the contributions from different parameters. Also, data other than surface seismic data, such as well logs and checkshots, can also be helpful in further constraining the problem. This will be investigated in the near future.

ACKNOWLEDGMENT

We thank James Berryman for fruitful discussion about the theory and the choice of the synthetic model.

REFERENCES

Biondi, B., 2007, Residual moveout in anisotropic angle-domain common-image gathers: Geophysics, **72**, S93S103.

———, 2008, Automatic wave-equation migration velocity analysis: **SEP-134**, 65–78.

Biondi, B. and W. Symes, 2004, Angle-domain common- image gathers for migration velocity analysis by wavefield- continuation imaging: Geophysics, **69**, 12831298.

Cai, J., Y. He, Z. Li, B. Wang, and M. Guo, 2009, TTI/VTI anisotropy parameters estimation by focusing analysis, Part I: Theory: SEG Expanded Abstracts, **28**.

Claerbout, J. F., 1971, Towards a unified theory of reflector mapping: Geophysics, **36**, 467–481.

Fei, T. W. and C. L. Liner, 2008, Hybrid Fourier finite-difference 3D depth migration for anisotropic media: Geophysics, **73**, S27.

Fletcher, R., X. Du, and P. J. Fowler, 2009, Stabilizing acoustic reverse-time migration in TTI media: SEG Expanded Abstracts, **28**.

Guerra, C., Y. Tang, and B. Biondi, 2009, Wave-equation tomography using image-space phase-encoded data: SEP-report, **138**, 95.

Helbig, K., 1956, Die ausbreitung elastischer Wellen in anisotropen Medien: Geophys. Prosp., **04**, 70–81.

McCollum, B. and F. Snell, 1932, Asymmetry of sound velocity in stratified formations: Physics – A Journal of General and Applied Physics, **2**, 174–185.

Postma, G. W., 1955, Wave propagation in a stratified medium: Geophysics, **20**, 780–806.

Sava, P., 2004, Migration and velocity analysis by wavefield extrapolation: PhD thesis, Stanford University.

Sava, P. and B. Biondi, 2004a, Wave-equation migration velocity analysis-I: Theory: Geophysical Prospecting, **52**, 593–606.

———, 2004b, Wave-equation migration velocity analysis-II: Examples: Geophysical Prospecting, **52**, 607–623.

Shan, G., 2009, Optimized implicit finite-difference and Fourier finite-difference migration for VTI media: Geophysics, WCA189WCA197.

Shen, P., 2004, Wave-equation Migration Velocity Analysis by Differential Semblance Optimization: PhD thesis, Rice University.

Shen, P. and W. W. Symes, 2008, Automatic velocity analysis via shot profile migration: Geophysics, **73**, VE49–VE59.

Tang, Y. and R. G. Clapp, 2006, Selection of reference anisotropic parameters for wavefield extrapolation: SEP-report, **124**.

Tarantola, A., 1984, Inversion of seismic reflection data in the acoustic approximation: Geophysics, **49**, 1259–1266.

Woodward, M. J., 1992, Wave-equation tomography: Geophysics, **57**, 15–26.

Yuan, J., X. Ma, S. Lin, and D. Lowrey, 2006, P-wave tomographic velocity updating in 3D inhomogeneous VTI media: SEG Expanded Abstracts, **25**.

Zhang, Y. and H. Zhang, 2009, A stable TTI reverse time migration and its implementation: SEG Expanded Abstracts, **28**.

Zhou, H., D. Pham, and S. Gray, 2004, Tomographic velocity analysis in strongly anisotropic TTI media: SEG Expanded Abstracts, **23**.

Zhou, H., D. Pham, S. Gray, and B. Wang, 2003, 3-D tomographic velocity analysis in transversely isotropic media: SEG Expanded Abstracts, **22**.